Soft Matter

Self-assembly of Donor-acceptor Conjugated Polymers Induced by Miscible 'Poor' Solvents

Journal:	*Soft Matter*
Manuscript ID	SM-ART-12-2018-002517.R1
Article Type:	Paper
Date Submitted by the Author:	12-Jan-2019
Complete List of Authors:	Xi, Yuyin; University of Washington, Chemical Engineering Wolf, Caitlyn; University of Washington, Chemical Engineering Pozzo, Danilo; University of Washington, Chemical Engineering

Self-assembly of Donor-acceptor Conjugated Polymers Induced by Miscible 'Poor' Solvents

Yuyin Xi†, Caitlyn M. Wolf, and Lilo D. Pozzo*

Department of Chemical Engineering, University of Washington, Seattle, WA 98195

* Email: dpozzo@uw.edu

† Current address:

Center for Neutron Research, National Institute of Standards and Technology, Gaithersburg, MD, 20899, USA

Department of Chemical and Biomolecular Engineering, University of Delaware, Newark, DE, 19716, USA

Abstract

The solution-phase self-assembly of donor-acceptor conjugated polymer (DACP) poly[2,5-(2-octyldodecyl)-3,6-diketopyrrolopyrrole-alt-5,5-(2,5-di(thien-2-yl)thieno [3,2b]thiophene (DPPDTT), is demonstrated and investigated from binary solvent mixtures. It is found that the polarity of a miscible 'poor' solvent (e.g. methanol, dimethyl sulfoxide), which is added to a stable polymer solution in chloroform (i.e. 'good' solvent), strongly affects the resulting nanostructure. Nanoribbons are formed by the addition of certain polar (e.g. methanol) 'poor' solvents to the mixture, while amorphous aggregates are formed upon addition of non-polar 'poor' solvent, such as n-hexane. Atomic force microscopy (AFM), scanning transmission electron microscopy (sTEM) and small angle neutron scattering (SANS) are used to characterize the shape and size of the nanostructures. Experiments show complex self-assembly in solution occurs for DACPs when compared to conjugated homopolymers. SANS results also provide quantitative analysis of DACP

conformations in solution before self-assembly occurs. The addition of different polar 'poor' solvents could also alter the size of the assembled nanostructures, as well as the fraction of polymers that self-assemble. The surface orientation and the crystal structure of the nanostructures is also probed by grazing-incidence wide-angle x-ray scattering (GIWAXS). Organic field effect transistors (OFETs) are used to characterize charge transport properties for nanoribbons where enhancement of the average hole mobility is observed.

Introduction

Conjugated polymers (CPs) have gained interests due to their potential to be used in electronic devices, such as flexible and stretchable electronic skin, light weight and economic organic photovoltaics (OPVs), electrically controllable and scalable smart windows, and biocompatible electronics mimicking neural systems.[1–4] However, limited charge transport is still a major hindrance for most CP devices in comparison to inorganic counterparts.

Thanks to effective molecular design, donor-acceptor CPs (DACPs) with alternating electron-rich units (donor) and electron-deficient units (acceptor) covalently bonded within the same chain are emerging as excellent candidates to realize high mobilities (>10 cm^2/V-s). [5,6] Examples are poly[4-(4,4-dihexadecyl-4H-cyclopenta[1,2-b:5,4-b′]dithiophen-2-yl)-alt-[1,2,5]- thiadiazolo[3,4-c]pyridine] (PCDTPT) with a carrier mobility of 21.3 cm^2/V-s and poly[2,5-(2-octyldodecyl)-3,6-diketopyrrolopyrrole-alt-5,5-(2,5-di(thien-2-yl)thieno [3,2b]thiophene (DPPDTT) with a carrier mobility of 19.5 cm^2/V-s. [5–7] Besides showing excellent electrical performance, light harvesting efficiency of OPVs have also benefited from these types of polymers because of a lower bandgap.[8] It is worth mentioning that the demonstrated high electrical performance often involves carefully controlled processing of the polymers.[5,6] This is because conjugated polymers have multiple

degrees of freedom and may form structures that interrupt charge transport. [9] Forming long and well-organized structures with close inter-chain packing, for example by π-π stacking, is an effective way to enhance conductivity. [10] Therefore, inducing the formation of such structures in DACPs is of great interest for high performance organic electronic devices. [11–15]

Solution-based nanowire or 'whisker' self-assembly is one of the most widely used methods to induce the formation of structures with long range order in homopolymer CPs (e.g. Poly(3-hexylthiophene) (P3HT)). By tuning the quality of solvents, nanofibers or nanoribbons can be formed for P3HT and many other poly(3-alkylthiophenes). [16–18] The shape of the assembled structure depends on the solvent quality, the kinetics of self-assembly and the polymer concentration among other parameters. [16–18] 'Poor' solvent addition has also been demonstrated to be effective and well-controlled self-assembly method. So far, many 'poor' solvents have been investigated to promote nanofiber formation, including acetone, [19] anisole, [20] cyclohexanone, [21] ethyl acetate, [22] hexane, [23] n-butylbenzene, [24] dodecane, [13] tetrahydrofuran (THF), [25] and methylene chloride (MC). [26] For P3HT, it is proposed that once the solubility limit is reached, nanofibers can form. [23] However, limited work has focused on controlling the assembled structures by systematically changing 'poor' solvents.[11]

In polymer solutions, the relative strength of polymer-polymer and polymer-solvent interactions determines whether they stay in a fully dissolved conformation or in an aggregated state. [23] Understanding polymer conformation in solution is of vital importance because it determines their crystallization behavior and the electrical, mechanical, and optical properties. [27] Small angle neutron scattering (SANS) is a great technique to non-destructively extract ensemble-averaged molecular information and structure with high resolution over multiple length scales. It was also used to provide precise analysis of the rigidity of CP chains (i.e. Kuhn length) in fully dissolved

states. [27,28] This information is essential to correlate changes in molecular architecture to solution and solid-state structure. However, to the best of our knowledge, SANS has not yet been applied to quantify the stiffness or solution conformation of donor-acceptor conjugated polymers (DACPs). This same technique can also be utilized to determine the dimensions of nanostructures, polymer fractions that self-assemble, and the fractal dimension of networks of CPs. [11,13,14,30] Work in our group has also investigated the effect of solvent quality on both self- and directed- assembly of homopolymers such as P3HT and poly(9,9-dioctylfluorene) (PFO)) using SANS. [13,14,29,30]

Compared to homopolymers like P3HT, controlling the self-assembly of DACPs has proven to be challenging due to the complex molecular structure of the polymer backbone. For example, several minimum energy inter-chain packing states may exist for just one DACP. [31–34] The heterogeneous arrangement of donor and acceptor subunits within the same chain will also likely change polymer-polymer and polymer-solvent interactions in dissolved states. Polymer-polymer interactions are largely affected by the molecular structure of chains as determined through synthesis. Molecular weight, backbone curvature, side chain positions and bulkiness are all found to affect self-assembly. [35] Controlling polymer-solvent interactions, however, has not yet gained traction as a strategy to induce self-assembly in DACPs. For any given polymer, by choosing optimum polymer-solvent pairs, one may achieve desired structures and properties. Few works have reported on the formation of whiskers or other dispersed structures for DACPs in different solvents. Chen et al. discovered that hole mobility of a diketopyrrolopyrrole (DPP) polymer with branched side chains (PDPP3F-BO) could be further enhanced by about 1.5 times after mixing 30 v% methanol into DACP solutions. [36] They ascribe this result to a reduced π-π stacking distance and a more favorable in-plane orientation in the substrate after coating. Zheng et al. reported the formation of 1-D rod-like structures for benzodifurandione oligo(*p*-phenylene vinylene) DACP polymer (BDOPV-2T)

in ‘good’ solvents and a 2-D lamellar structure in ‘poor’ solvents. Using solvent mixtures leads to an enhancement of both crystallinity and interconnectivity, resulting in electron mobility improvements from 1.8 cm^2/V-s to 3.2 cm^2/V-s. [32] Moreover, polar co-solvents, in comparison to nonpolar solvents, are reported to achieve almost one order of magnitude in enhancement of power conversion efficiency (PCE) in OPVs due to the formation of small aggregate sizes. [37]

Here, we present a systematic structural investigation on the effect of solvent mixtures on the formation of self-assembled structures for DACPs. Our aim is to provide insights into structure engineering strategies to optimize solution-processing strategies and properties of DACPs. DPPDTT is chosen as a model system for this study because it exhibits a high charge carrier mobility and extraordinary stability at ambient environmental conditions, which is often deficient in many CPs. No degradation is observed for OFETs based on this polymer after switching on and off for more than 3500 cycles and its high electrical performance can be maintained for over a year in ambient air. [6,15]

Experimental

Materials:

DPPDTT was purchased from Ossila (Sheffield, UK), while PCDTPT and Poly[(5-fluoro-2,1,3-benzothiadiazole-4,7-diyl)(4,4-dihexadecyl-4H- cyclopenta[2,1-b:3,4- b']dithiophene-2,6-diyl)(6-fluoro-2,1,3-benzothiadiazole-4,7-diyl)(4,4-dihexadecyl-4H cyclopenta [2,1-b:3,4-b']dithiophene-2,6-diyl)] (PFT-100) were obtained from 1-Material (Quebec, Canada). Poly[N-9′-heptadecanyl-2,7-carbazole-alt-5,5-(4′,7′-di-2-thienyl-2′,1′,3′ benzothiadiazole)] (PCDTBT) was acquired from Sigma-Aldrich (St. Louis, MO, USA). Detailed information of the polymers, including batch numbers, molecular weight (Mw) and dispersity (*Đ*) is listed in Table S1 in the supporting information. Trichloro(decyl)silane (DTS) was purchased from Gelest

(Morrisville, PA, USA). Hydrogenated solvents: chloroform, methanol, dimethyl sulfoxide (DMSO), isopropanol (IPA), n-hexane, and acetonitrile (ACN) were purchased from Sigma-Aldrich. Acetone and toluene were obtained from Fisher Scientific (Hampton, NH, USA). Deuterated solvents: d-chloroform, d4-methanol, d6-dimethyl sulfoxide, and d3-acetonitrile were purchased from Cambridge Isotope Laboratories (Tewksbury, MA, USA). All chemicals were used as received without further purification. Mechanical grade silicon wafers were obtained from University Wafer (South Boston, MA, USA). Heavily n-doped silicon wafers with 200 nm thermally grown oxide were acquired from WRS Materials (Vancouver, WA, USA). Chromium rods and gold pellets used for evaporation were purchased from RD Mathis company (Long Beach, CA, USA).

Sample preparation:

DPPDTT, PCDTBT, and PFT-100 were first dissolved in chloroform at 60 °C, which is considered to be a 'good' solvent for all polymers. The initial polymer concentration in chloroform was adjusted accordingly for all samples to keep the final concentration at 1.6 mg/ml after mixing with the co-solvents at variable ratios. All of the solvent ratios that are stated in this work correspond to volume percentage. Due to the high solubility of PCDTPT, it does not self-assemble at 1.6 mg/ml with the same volume ratio of 'poor' solvents at room temperature. Therefore, the final concentration of polymer had to be adjusted to 3.2 mg/ml to compare the resulting structures. After full dissolution in chloroform, a specific co-solvent (i.e. methanol, n-hexane, dimethyl sulfoxide (DMSO), acetonitrile (ACN), isopropanol, or acetone) was slowly added to the polymer solution. The solvent was added gently so that the 'poor' solvents were initially phase-separated as a new layer sitting on top of chloroform. By slightly shaking the samples, the two layers would mix to form a homogeneous solution. Figure S1 in the supporting information shows the formation of two

solvent layers after methanol is gently added and how homogeneous solutions form after shaking. Large polymer aggregates formed instantaneously at the interface of the two solvents. To make a dispersible solution, samples were immersed for ~5 min in a sonication bath (Branson 5000, 40 kHz, 160W, Danbury, CT, USA).

Scanning Transmission Electron Microscopy (sTEM):

An FEI (Tecnai G2 F20, FEI company, Hillsboro, OR, USA) transmission electron microscope (TEM) was used to characterize the structures the polymer at various solvent mixtures. Due to the relatively low contrast for polymer samples, scanning mode was utilized to capture high resolution images. The solutions were diluted by 10 times in a solvent mixture with the same solvent ratio before characterization. For sample preparation, a volume of ~5 μl of the samples was drop-cast onto a pure carbon grid (200 mesh Cu, Ted Pella Inc., Redding, CA, USA) that was placed on top of filter paper to wick the excess solvent. The grid was left in a well-ventilated chemical hood to dry for at least one day in air.

Atomic Force Microscopy (AFM):

A Bruker Dimension Icon-PT atomic force microscope (AFM) was used to characterize the surface morphology of all polymer films in peak force tapping mode. The samples were prepared by spin coating polymer solutions onto a precut glass slide or SiO_2 surface that is thermally grown on a silicon wafer. A scan size of 2.5 μm by 2.5 μm was used for each image.

Grazing-incidence wide-angle x-ray scattering (GIWAXS):

GIWAXS experiments were performed at beamline 8-ID-E of the Advanced Photon Source at Argonne National Laboratory. [38] The polymer samples were prepared by drop casting ~100 µl of solution on a silicon substrate that was sequentially cleaned using acetone, IPA, and DI water in a sonication bath. The samples were dried in air for at least overnight. A beam size of 200 µm by 20 µm was used with an energy of 10.92 keV. The substrates were aligned with a tilt angle of 0.14˚ so that the x-ray beam would penetrate through the polymer layer and be reflected off from the polymer/silicon interface. A total of two frames were recorded with a vertical detector offset to form a full image. The two frames were combined together using GIXSGUI software to remove dark stripes from the x-ray detector. [39] Each frame was exposed for 10 s for every sample. GIXSGUI was also used to reduce the 2-D pattern to a 1-D scattering profile in both out-of-plane and in-plane directions. [39]

Small angle neutron scattering (SANS):

SANS experiments were conducted at the NIST Center for Neutron Research (NCNR, Gaithersburg, Maryland). Both NG7 and NGB-30 were used for characterization of polymer solutions. [40] Standard configurations with three detector positions were used and the 1-D profiles were stitched together to cover a q range of 0.0033 $Å^{-1}$< q <0.45 $Å^{-1}$. The experiments utilized sample cells with either 1 mm path length (NG7) or 2 mm path length (NGB-30) without any influence on the results. Quartz windows were held together by the titanium cells and sealed by Teflon coated o-rings. All the samples were prepared fresh on-site and the scattering experiment was performed within the same day of preparation. Every polymer solution for SANS experiments was prepared in deuterated solvents to enhance the contrast of the polymers and to reduce the incoherent background. Scattering profiles for quartz windows were recorded for every sample to

account for the scattering of the empty cell and to subtract the background precisely. All pure solvent mixtures were measured alone to separate the scattering signal of droplets formed by solvent mixing from the scattering signal of polymers. Standard Igor (WaveMetrics, Inc., Lake Oswego, OR, USA) reduction macros were used to reduce the SANS data. [41] SASview software was then utilized to fit the data to an appropriate model. [42]

Organic field effect transistor (OFETs) fabrication:

OFETs devices were fabricated in a bottom gate bottom contact configuration. Standard photolithography processes were used to define a device active region of Lg=100 μm and Wg=1000 μm. Two layers of metal (10 nm Cr and 50 nm Au) were deposited over a wafer having a dielectric layer of 200 nm SiO_2 thermally grown on heavily n-doped silicon. The substrates were diced into chips 0.9 cm by 1 cm in size by a Disco dicing saw (DAD321, Tokyo, Japan) after coating a thin layer of photoresist for surface protection. The pre-patterned substrates were cleaned sequentially with acetone, IPA and DI water and blow dried in air. Then the surface was further cleaned by UV/ozone treatment for 20 min right before silane treatment to passivate the surface. Afterwards, the substrates were submerged in a solution of 1 v% of DTS in toluene at 60 ˚C for 30 min. Then they were rinsed with toluene and blow dried in air. The polymer solution was spin coated at 1500 rpm for 30s and dried in a nitrogen filled glovebox. In order to characterize the structures as formed in solution, no annealing was used after spin coating. The electrical characterization was conducted in a nitrogen filled glove box with a Signatone probe station (Gilroy, CA, USA). A Hewlett-Packard (Palo Alto, CA, USA) 4145B semiconductor parameter analyzer was utilized to record the current voltage curve.

Results:

DPPDTT was fully dissolved in chloroform at ~60 ˚C, and methanol was slowly added into the polymer solutions to induce assembly while keeping the final polymer concentration constant. At 15 v% methanol, large fibril aggregates visible by bare eyes formed instantly at the vicinity of the 'poor' solvent. A brief sonication would re-disperse those aggregates into a clear and uniform dispersion. With 20 v% methanol, much larger aggregates formed, which were still visible even after sonication. Figure 1 shows the AFM and sTEM images of polymer samples with varying ratios of methanol, which is a 'poor' solvent for DPPDTT. Compared to the morphology of samples processed from pure chloroform, the addition of 10 v% methanol increases the domain size. Starting at a higher ratio of 15 v% methanol, assembly into fibril structures is observed in both AFM and sTEM images. Further increasing methanol concentration to 20 v% produces wider and longer nanoribbons that appear to be flexible and superimposed over each other. The width of the nanoribbon varies from ~20 nm to above ~100 nm. It is important to note that uniform polymer films can only be prepared from spin coating at low methanol concentrations. Above 15 v%, the large aggregates formed in solution results in discrete islands on the substrate during spin coating. All the samples shown in Figure 1 were prepared within a couple hours after mixing the 'poor' solvent. The structures formed in solution at longer aging times for methanol concentrations of 20 v% (ribbons) and 10 v% (no ribbons) are shown in Figure S2 in the Supporting Information. For 10 v% methanol, no observable nanoribbons were formed even after 12 days of aging. In contrast, for 20 v% methanol concentration, the initially formed nanoribbons gradually grow larger in size and can be above 100 nm in width after 12 days aging in solution.

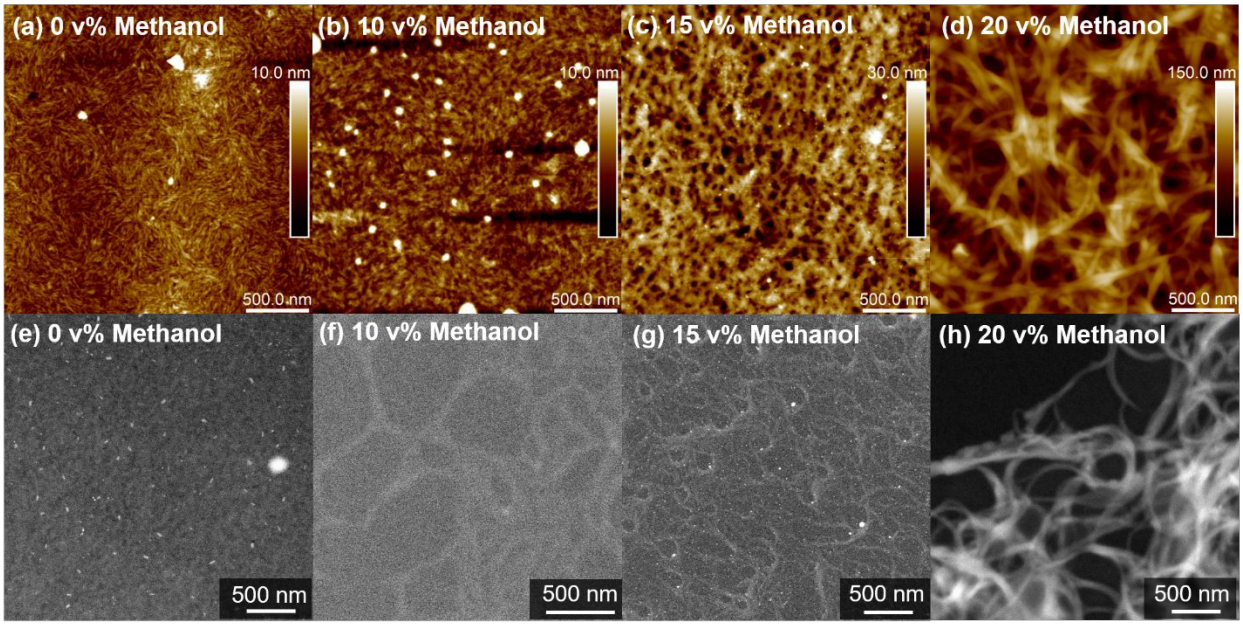

Figure 1. (a)~(d) AFM and (e)~(h) sTEM images of 1.6 mg/ml DPPDTT in chloroform mixed with (a) (e) 0 v% (b) (f)10 v% (c) (g) 15 v% and (d) (h) 20 v% Methanol.

Nanoribbons are clearly visible in solid films as probed by microscopy (Figure 1). However, a quantitative method to characterize polymer conformations and nanostructures in solution is also needed. This can eliminate artifacts that may occur from coating, drying and sample preparation. Figure 2 shows SANS profiles for the DPPDTT polymer in solvent mixtures of chloroform and methanol at various concentrations. The background scattering from pure solvents were subtracted from every sample by recording the scattering profile for each solvent mixture. The scattering profiles never show a plateau at low-q, indicating a large size and very rigid conformation in solution, even before inducing self-assembly. This is due to both the long polymer chain (i.e. high molecular weight) and the stiff and planar molecular structures of the DACP backbones. At low methanol ratios (below 10 v%), the scattering profiles overlap on top of each other, which suggests that no solution assembly occurs. At methanol concentrations higher than 15 v%, the scattering intensity increases in the low q-region and a clear hump develops at methanol concentrations of 20 v%, which correlates to the formation of nanoribbons.

To obtain quantitative conformational information, a semi-flexible cylinder model is used to fit the dissolved polymer chains in solution. [43,44] It is important to note that this model is only applicable to the dissolved chains before self-assembly. Once these form nanoribbons or nanofibers, a different shape-factor model (e.g. parallelepiped) needs to be added and used to extract structural parameters. In the semi-flexible cylinder model, the contour length, Kuhn length and cylinder radius are left as adjustable variables. Although the contour length can be determined if the monomer size and molecular weight of the polymer are known, it was still left as a variable because it is possible that a few polymer chains could possibly bind along the chain length direction and effectively increase the length of dissolved chain complexes as probed by SANS. Using the size of the repeat units and the molecular weight measured from gel permeation chromatography (GPC), the contour length of the polymer is estimated to be ~141 nm. [34] Figure 2 (b) compares fit parameters as obtained from SANS. The contour length is roughly constant at ~120 nm until methanol concentrations exceed 10 v%. At 15 v% methanol, an abrupt increase in the length is observed, indicating the onset of self-assembly to larger structures. Similar trends apply to the radius since gradual addition of methanol induces an increase in the cross-sectional size of the cylinder. The Kuhn length decreases when polymers start to form larger structures.

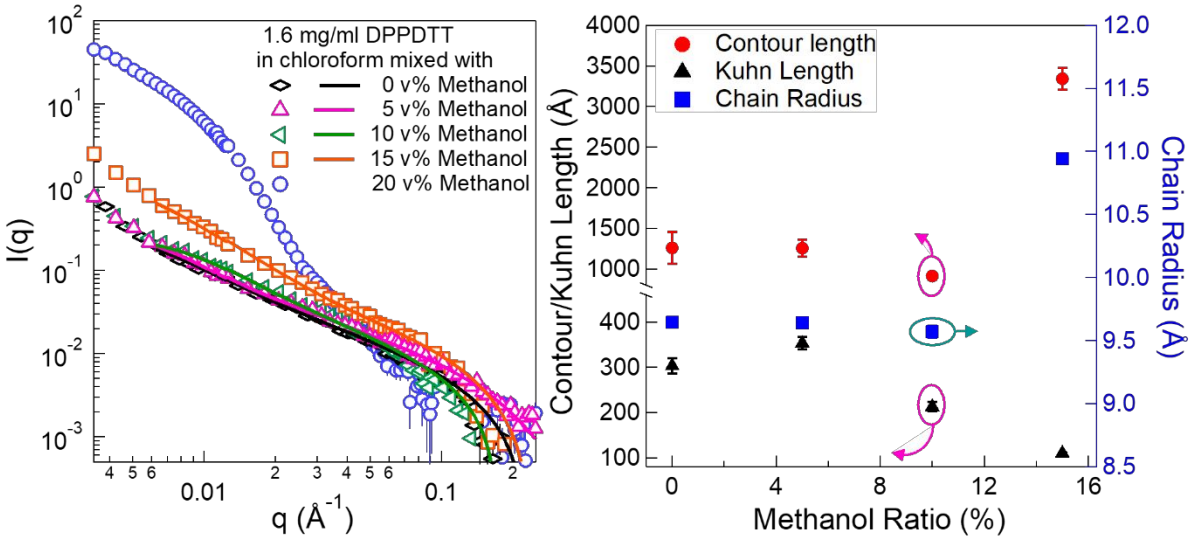

Figure 2. (a) SANS profiles for 1.6 mg/ml DPPDTT in chloroform mixed with various amounts of methanol. The data for samples with 0 v% to 15 v% methanol is fit using a semi-flexible cylinder model. (b) Extracted values for contour length, Kuhn length, and radius of the cylinder as a function of methanol concentration.

In sharp contrast, the addition of the non-polar solvent n-hexane (ε=2), which is also a 'poor' solvent for DPPDTT, to polymer solution in chloroform, does not lead to nanoribbon formation. Figure 3 (a) shows AFM images of the resulting films after addition of 20 v% n-hexane. No nanoribbons formed even after the addition of up to 50 v% n-hexane. Instead, the addition of non-polar 'poor' solvents results in large aggregates with amorphous shapes. The diameter of the aggregates increases with the n-hexane content in the solvent, which ranges from tens of nanometers to a few hundred nanometers. In contrast to these results, the addition of n-hexane would promote the formation of nanofibers for homopolymer poly(3-hexylthiophene) (P3HT) in chloroform or other 'good' solvents. [17,23]

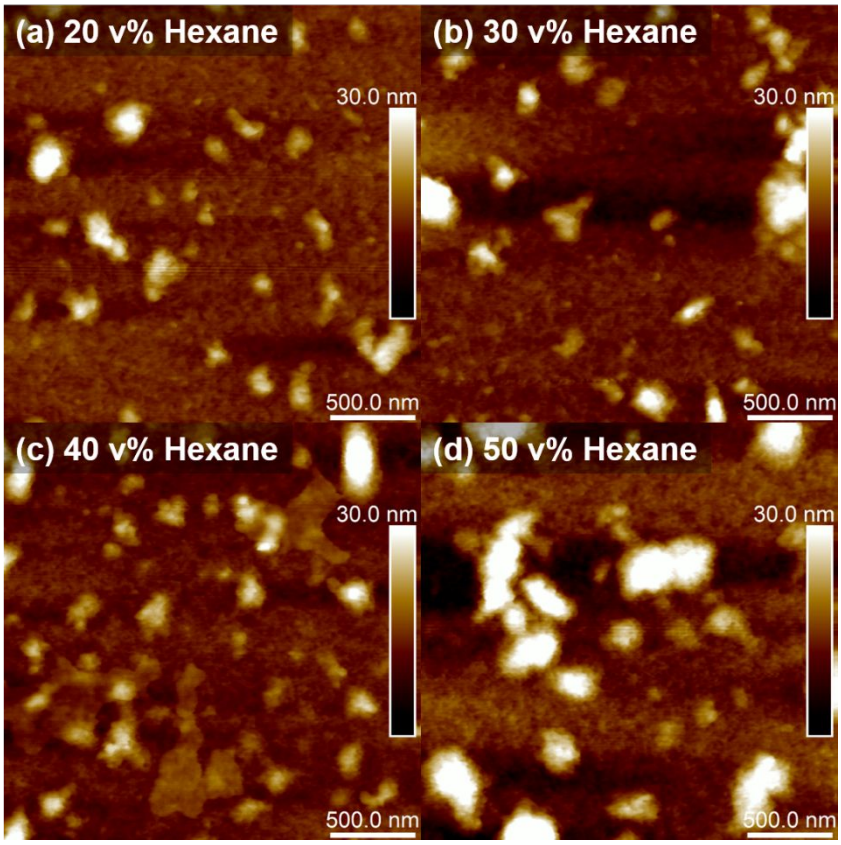

Figure 3. AFM images of spin coated films of 1.6 mg/ml DPPDTT in chloroform mixed (a) 20 v% (b) 30 v% (c) 40 v% and (d) 50 v% n-hexane.

While the formation of nanofibers and/or nanoribbons is typically indicative of a well-ordered chain arrangement, it is still important to analyze the crystalline structure and polymer packing using high resolution methods. Grazing-incidence wide-angle x-ray scattering (GIWAXS) was utilized to probe polymer samples prepared from chloroform mixtures with methanol (polar) and n-hexane (non-polar) 'poor' solvents in Figure 4. The polymer chain orientation with respect to the substrate can be characterized by the azimuthal intensity distribution for crystalline peaks along different angles from the 2-D profiles. The intensity distribution of the π-π stacking peak at 1.7 $Å^{-1}$ shows that the 'face-on' orientation was favorable in pure chloroform samples. In contrast, the addition of 20 v% n-hexane increased the 'edge-on' orientation while still maintaining a fairly

strong scattering signal at the out-of-plane direction. Samples processed from pure chloroform and from chloroform : n-hexane mixtures show bimodal arrangement of π-π stacking peaks, indicating the coexistence of both chain orientations (i.e. 'face-on' and 'edge-on') as shown in Figure 4 (b). However, in samples prepared from pure chloroform and from chloroform with 20 v% n-hexane, the 'edge-on' π-π stacking peaks are more defined in the in-plane direction (horizontal) as compared to out-of-plane direction (vertical). In sharp contrast, samples prepared from chloroform with 20 v% added methanol (Figure 4 (c)) show a nearly uniform distribution of the intensity of the π-π stacking peak along all azimuthal angles. This is attributed to the formation of nanoribbons since the interconnected stiff structure leads to a random or isotropic distribution of fiber orientations with π-π stacking peaks oriented in nearly all directions.

By integrating along both out-of-plane (Figure 4 (d)) and in-plane (Figure 4 (e)) directions, the peak positions and relative peak intensities were also compared. In Figure 4 (d), the intensity of the peak at 1.37 $Å^{-1}$ was greatly enhanced as compared to the π-π stacking peak at 1.7 $Å^{-1}$ when n-hexane was used. The intensities of those two peaks were comparable to each other for both pure chloroform and for samples with 20 v% added methanol. The peak at 1.37 $Å^{-1}$ was found to be strongly correlated to the distance between two interdigitated side chains by comparing to molecular dynamics simulation. [33] This means that the addition of n-hexane possibly affects the side-chain packing.

Another interesting change is the emergence of two new scattering peaks at 2.2 $Å^{-1}$ and 3.2 $Å^{-1}$ for the sample with 20 v% methanol that do not show up in samples coated from either pure chloroform or from mixtures with 20 v% n-hexane. The peak at 3.2 $Å^{-1}$ is not shown in Figure 4, but it is visible in Figure S3 in the Supporting Information. The relative intensity of this peak increases as a function of aging time, which is shown in Figure S3 (f) ~(k) in the Supporting

Information. It was determined that these peaks did not originate from the substrate (i.e. different q position) or from the scattering instrument. Instead, it was concluded that metal nanoparticles were slowly forming from residual catalyst contaminants (Pd ions) reacting with some of the co-solvents (e.g. methanol) and leading to x-ray scattering peaks at 2.2 $Å^{-1}$ and 3.2 $Å^{-1}$. sTEM images also show nanoparticle formation with addition of these polar 'poor' solvents (Figure S4 in the Supporting Information). It is important to note that the residue catalyst may potentially affect the scattering profiles in future experiments, which could be addressed by additional purification steps of polymers. However, considering catalyst nanoparticles with different X-ray scattering peak positions, small particle size, low concentration, and negligible scattering contrast in solutions, it was concluded that the generation of nanoparticle does not affect or interfere with polymer scattering for both GIWAXS and SANS data in the current study. More detailed discussions can be found in the Supporting Information.

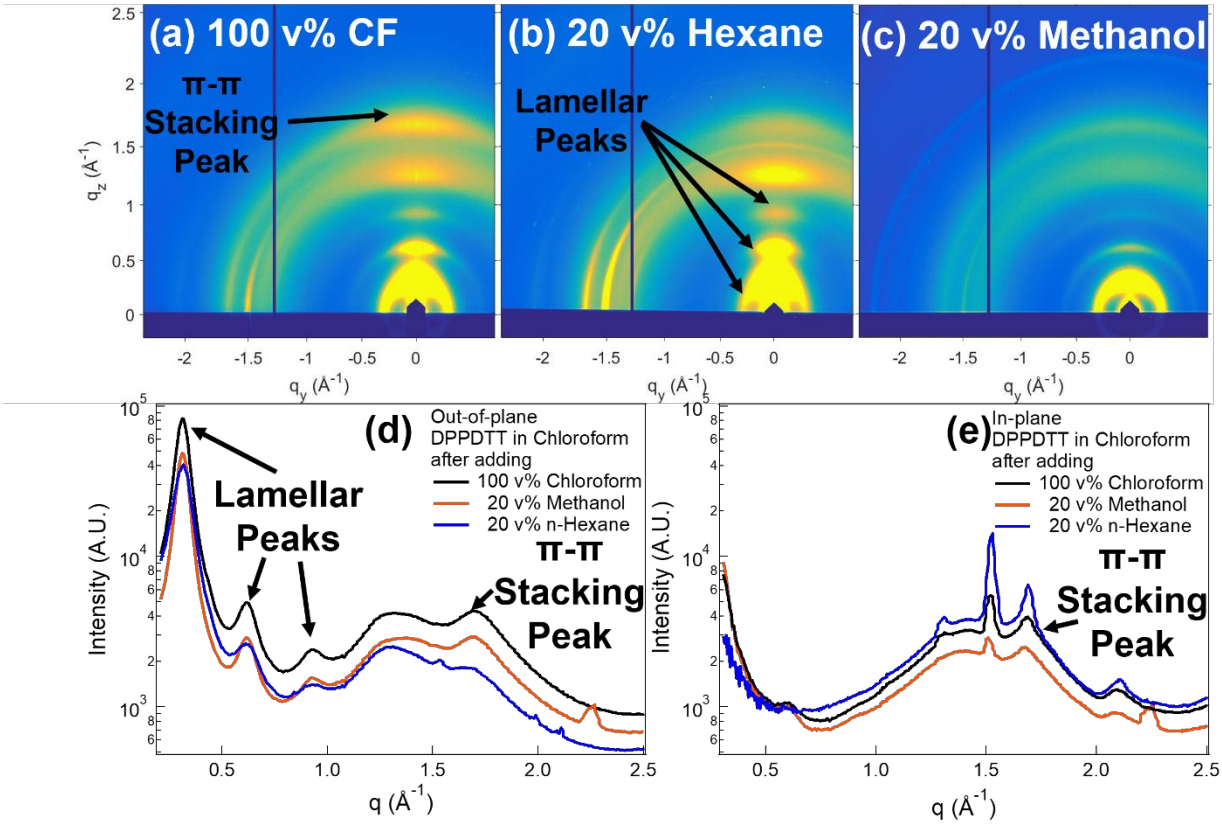

Figure 4. 2D GIWAXS pattern of film drop-cast from 1.6 mg/ml DPPDTT in (a) pure chloroform and with (b) 20 v% n-hexane (non-polar) and (c) 20 v% methanol (polar) 'poor' solvent addition. 1D GIWAXS intensity integration (d) out-of-plane (φ=105°) and (e) in-plane (φ=175°) for the three samples with a 5° integration angle.

The differences in both nanostructure and polymer packing that is caused by solvent polarity motivated the exploration of other commonly used organic 'poor' solvents, including DMSO (ε=47), ACN (ε=37.5), acetone (ε=20), and IPA (ε=17). The measured dielectric constant of different 'poor' solvents with various ratios are shown in Figure S5 in the supporting information. Nanoribbon formation can be clearly observed in samples containing DMSO and ACN after 10 days of aging in Figure 5 (a) and (b). The samples without aging are shown in Figure S6 in the Supporting Information, which also presented nanoribbon formation with the addition of polar

'poor' solvents. The cross-sectional size of these nanoribbons is on the order of tens of nanometers and the length can extend to a few micrometers. Compared to the above two solvents, IPA and acetone, which have dielectric constants around 20 and are less polar than methanol (ε=32), did not show clear signs of nanoribbon formation. In order to ensure that enough supersaturation was induced by the addition of IPA and acetone, higher solvent ratios were also prepared and their AFM images are shown in Figure S7 in the Supporting Information. With 30 v% of IPA, nanoribbons were also generated. However, samples with acetone did not produce nanoribbons even at concentrations of up to 40 v%. Instead, large aggregates are visible under AFM (Figure S7 in the Supporting Information). Based on the above results, a critical dielectric constant between ε=20 and ε=32 seems to be necessary for the added 'poor' solvents to induce the formation of nanoribbons.

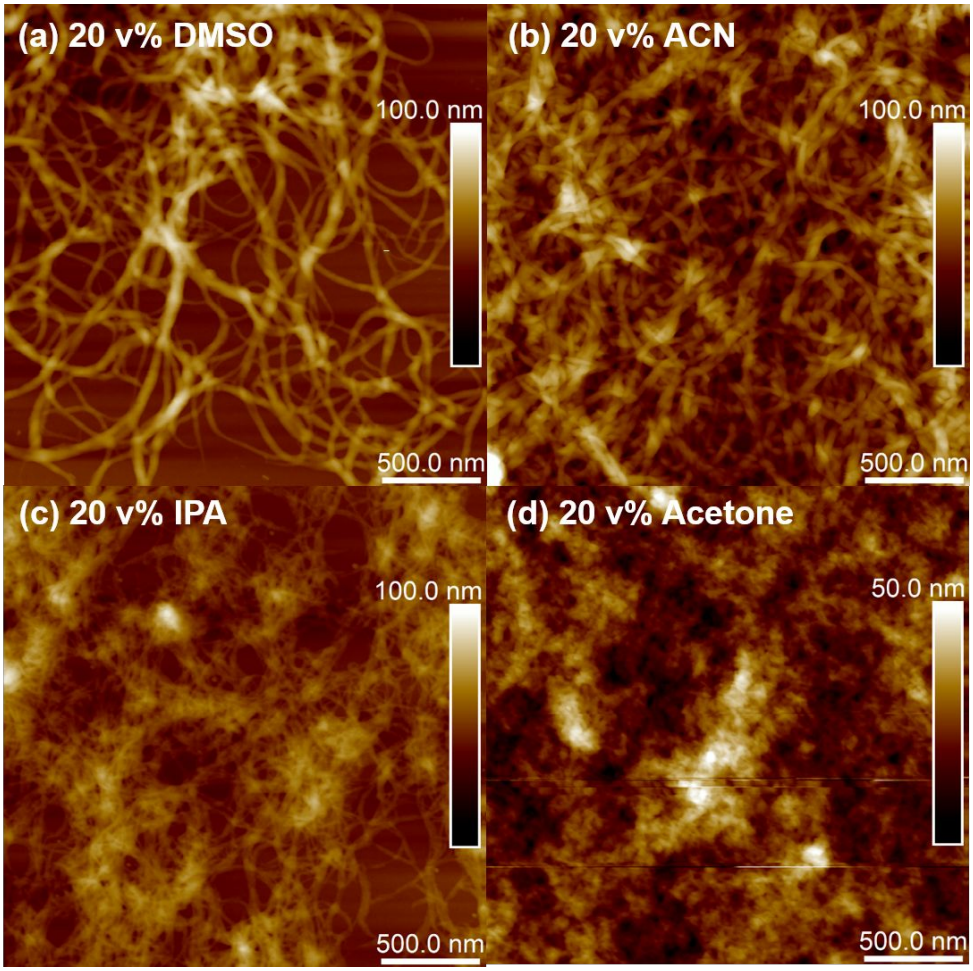

Figure 5. AFM images of 1.6 mg/ml DPPDTT in chloroform mixed with 20 v% (a) DMSO (b) Acetonitrile (ACN) (c) IPA (d) Acetone. The samples were casted after aging for 10 days in solution.

To further quantify the size of nanoribbons, SANS was also used on samples prepared from other polar 'poor' solvents (i.e. ACN, and DMSO). The scattering profiles are shown in Figure 6 along with reference samples that were prepared in pure chloroform. A combined model of long parallelepiped fibers [45,46] and dissolved polymers [47,48] was used to fit the data in order to obtain the cross-sectional dimensions and the total amount of polymers that formed nanoribbons in the chloroform-solvent mixtures. This model was previously implemented to characterize the size of P3HT nanofibers in solution. [11,14,49] When polymers are fully dissolved in samples with low

methanol concentrations (below 15 v% shown in Figure 2) a single model of semi-flexible cylinders can be applied to model the chain conformation. However, when conditions are adequate for self-assembly to occur, such as for samples in chloroform with 20 v% methanol, DMSO, or ACN the scattering includes a combination of form-factors (i.e. shape functions) from the assembled nanoribbons (i.e. parallelepiped model) and from the remaining 'free' dissolved polymer (i.e. dissolved polymer model with excluded volume effect) that exist in equilibrium. A detailed description of the model can also be found in the supporting information. The width and thickness of nanoribbons, as well as the fraction of the total polymer that was forming nanoribbons were the only fit variables. The rest of the parameters were constrained to known values.

The fit results are summarized in Table 1. The nanoribbons formed in ACN and DMSO were very similar in size, with cross-sectional thickness (parameter 'a') of ~10 nm and width (parameter 'b') of ~25 nm. In contrast, the nanoribbons formed in methanol were substantially larger with both dimensions almost doubled. This result was further corroborated by comparing AFM images of Figure 1 (d) and with Figure 5 (a) and (b). Even though nanoribbons were generated in different polar solvents, the size of ribbons induced in mixtures of chloroform and methanol was different from the others. Besides the cross-sectional size of the nanoribbons, the fraction of polymers that assembled also varied from solvent to solvent. This fraction correlated well with the polarity of the 'poor' solvents. Almost 80% of polymers formed nanoribbons in DMSO (ε=47) and ~ 66% of polymer chains assembled into ribbons upon addition of ACN (ε=37.5). Methanol, with the lowest dielectric constant of the three (ε=32), caused the assembly of the lowest amount of polymer into nanoribbons.

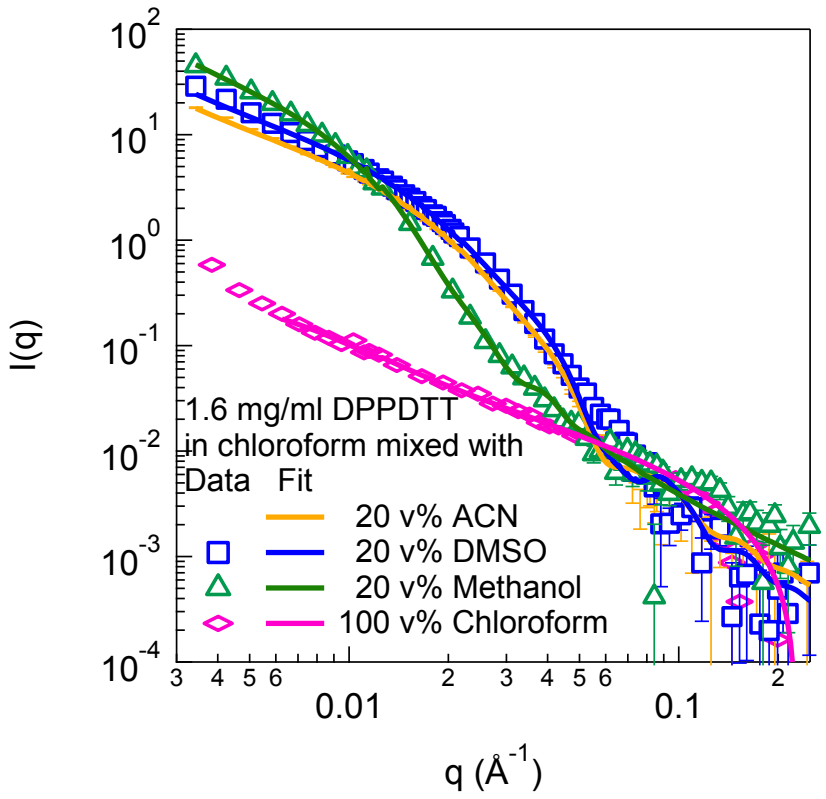

Figure 6. 1D SANS profiles of nanoribbons formed in chloroform with added 20 v% ACN, 20 v% DMSO, and 20 v% methanol. The scattering profiles were fit with a combined model of parallelepiped and dissolved polymer with excluded volume effects. [45–48] The fit for the sample prepared in chloroform with 20 v% methanol included polydispersity in the height of the cross-section 'a' into consideration. The scattering profile of fully dissolved polymers in pure chloroform is also added for comparison along with the fit to a semi-flexible cylinder model.

Table 1. Cross-sectional dimensions (a, b) of nanoribbons extracted from fits, dielectric constant (ε) of 'poor' solvents and the fraction of polymer chains that were located in the nanoribbons.

'Poor' solvent	a (nm)	b (nm)	Dielectric Constant (ε)	Polymer Fraction in Nanoribbons (%)
20 v% DMSO	9.8	25.2	47	77.3
20 v% ACN	10.2	23.5	37.5	66.5

20 v% Methanol	23.2	40.8	32	39.5

GIWAXS was again used to characterize the chain packing for samples from these other 'poor' solvents. The 2D scattering patterns and 1D integration profiles are shown in Figure 7. Similar to samples prepared from chloroform with methanol (Figure 4), the π-π stacking peaks at 1.7 $Å^{-1}$ are uniformly distributed across the azimuthal angles when the polymers form nanoribbons (i.e. DMSO and ACN samples). This is again consistent with a random orientation of the nanoribbons with respect to the substrate. A comparison of the 1D integration profiles over the in-plane and the out-of-plane directions is shown in Figure 7 (e) and (f). In the out-of-plane direction, the π-π stacking peaks (q=1.7 $Å^{-1}$) show weaker scattering intensities compared to the peaks at q=1.37 $Å^{-1}$ for samples prepared from chloroform and the less-polar solvents, IPA and acetone. This is also observed for samples prepared from chloroform mixed with n-hexane in Figure 4 (d). In contrast, the relative intensity of the two peaks was similar for samples prepared from both DMSO and ACN. Additionally, the position of one of these peaks shifts from ~1.37 $Å^{-1}$ to 1.29 $Å^{-1}$ in mixtures with less-polar solvents, indicating a larger distance between side chains.

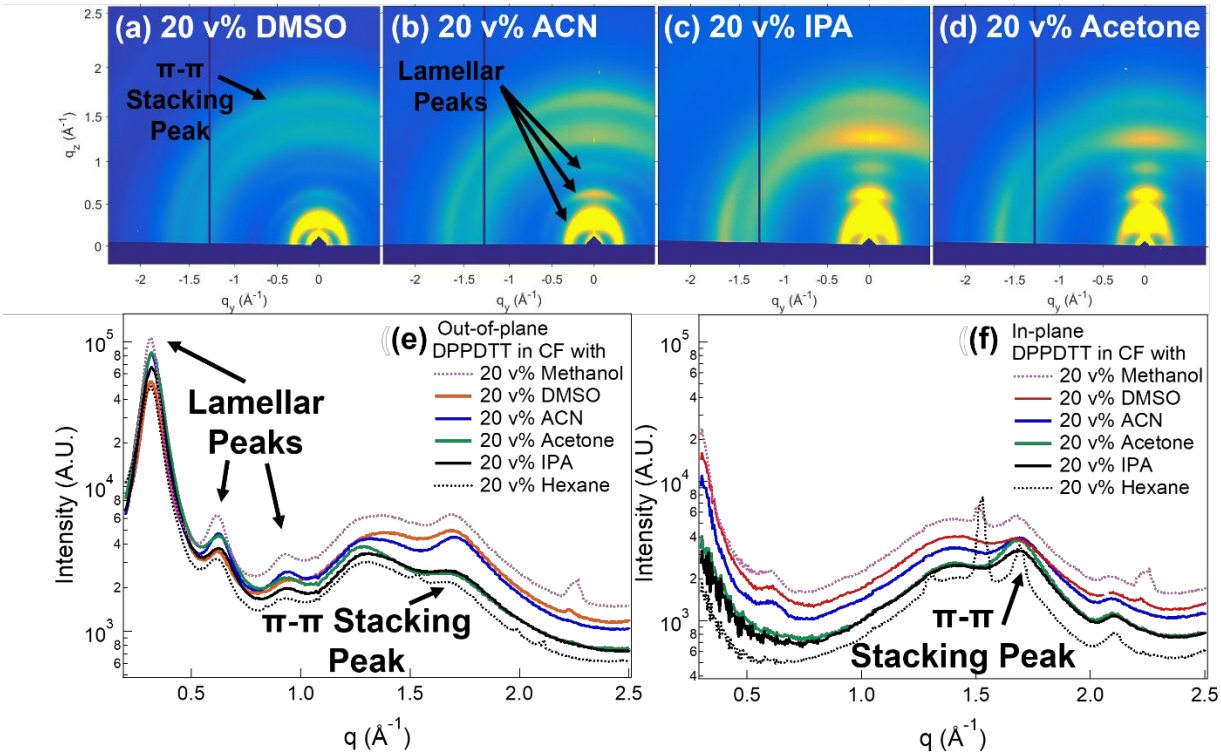

Figure 7. 2D GIWAXS pattern of films drop cast from 1.6 mg/ml DPPDTT in chloroform mixed with 20 v% (a) DMSO (b) Acetonitrile (ACN) (c) IPA (d) Acetone. (e) and (f) show the 1D integration in the out-of-plane (φ=105°) and in-plane (φ=175°) directions with a 5° integration angle, respectively. The dashed lines in each figure are the corresponding integration of polymer samples in chloroform mixed with methanol and n-hexane.

The electronic properties of nanoribbons were also investigated for samples prepared from mixtures of chloroform and methanol. Unfortunately, after the polymers were fully assembled into nanoribbons, it was difficult to form a uniform film using spin-coating due to the increased viscosity and elasticity. This was also documented for nanofibers formed from P3HT. [11] In order to gain insights into changes to the electrical properties that may be induced by formation of these structures, a high methanol content (15 v%) was used to induce partial ribbon assembly but kept low enough to achieve an adequate film quality during OFET fabrication. Based on SANS results in Figure 2, self-assembly starts to become evident at this solvent concentration. No annealing was

used during the fabrication process to ensure that the solution structure was maintained in the devices. The performance of these materials, as characterized by bottom gate bottom contact OFETs, is shown in Figure 8 (a). After self-assembly, the drain current increased by a factor of almost two at the same gate voltage when the channel is fully 'on'. A large hysteresis was observed for devices processed from pure chloroform but not in devices made with nanoribbons. This suggests that carrier traps are effectively reduced with the self-assembly of large ordered structures. Since the back sweep current is lower than the forward sweep current, the traps should be located close to the channel. [50]

In order to calculate the saturation mobility from the transfer curves, the data was replotted to show the square root of the current as a function of gate voltage (Figure 8 (b)). Two distinct slopes were observed under both conditions, which is very common for donor-acceptor conjugated polymers. [5–7,51] Significant efforts have been devoted to understanding the origin of this phenomena and it was recently proposed that reducing the contact resistance or using polymeric dielectric layers could help alleviate this effect. [52] It was also reported that this would be resolved when a very small gate length (5 μm) was used.[7] However, many of the literature-reported mobilities for DPPDTT have been extracted from analysis of the largest slope that is adjacent to the threshold voltage. This was recently considered to be an overestimation of the true mobility. [53]

In order to compare with published literature values and also to more accurately estimate the real mobility, we used two different methods to calculate the mobility. The first consists of an analysis of the largest slope, as has been done routinely in the literature for DPPDTT (dark dashed line in Figure 8 (b)). In addition, we also follow recent suggestions to calculate mobilities at high gate voltages (pink dashed line in Figure 8 (b)).[53] The results from both methods are summarized in Figure 8 (c) and an enhancement of mobilities for nanoribbons was observed in both analyses.

'High' represents the mobility obtained from fitting the largest slope of the curve close to threshold voltage and 'Low' is the more conservative estimation of the mobility from the high voltage slope shown as the dashed pink line. The averaged mobility of 10 devices, as estimated from the 'High' model fit, improves about 5 times after self-assembly was induced. The averaged value of the methanol 15 v% sample was ~3 $cm^2v^{-1}s^{-1}$ and highest mobility for one device was above 5 $cm^2v^{-1}s^{-1}$. Those values are comparable to the reported performance in recently published work for the same polymer but without any kind of annealing process.[54] Mobilities in that work were also calculated using the highest slope of the I-V curve. With the more conservative estimate, which is estimated from the 'low slope' of the region when the devices are completely turned 'on', the average mobility is about 0.13 $cm^2v^{-1}s^{-1}$, which is only slightly improved from samples processed from pure chloroform (0.097 $cm^2v^{-1}s^{-1}$). The output curves of devices in Figure 8 (d) showed significant enhancements in the drain current, thus an increase in 'on'/ 'off' ratio after self-assembly is induced by methanol.

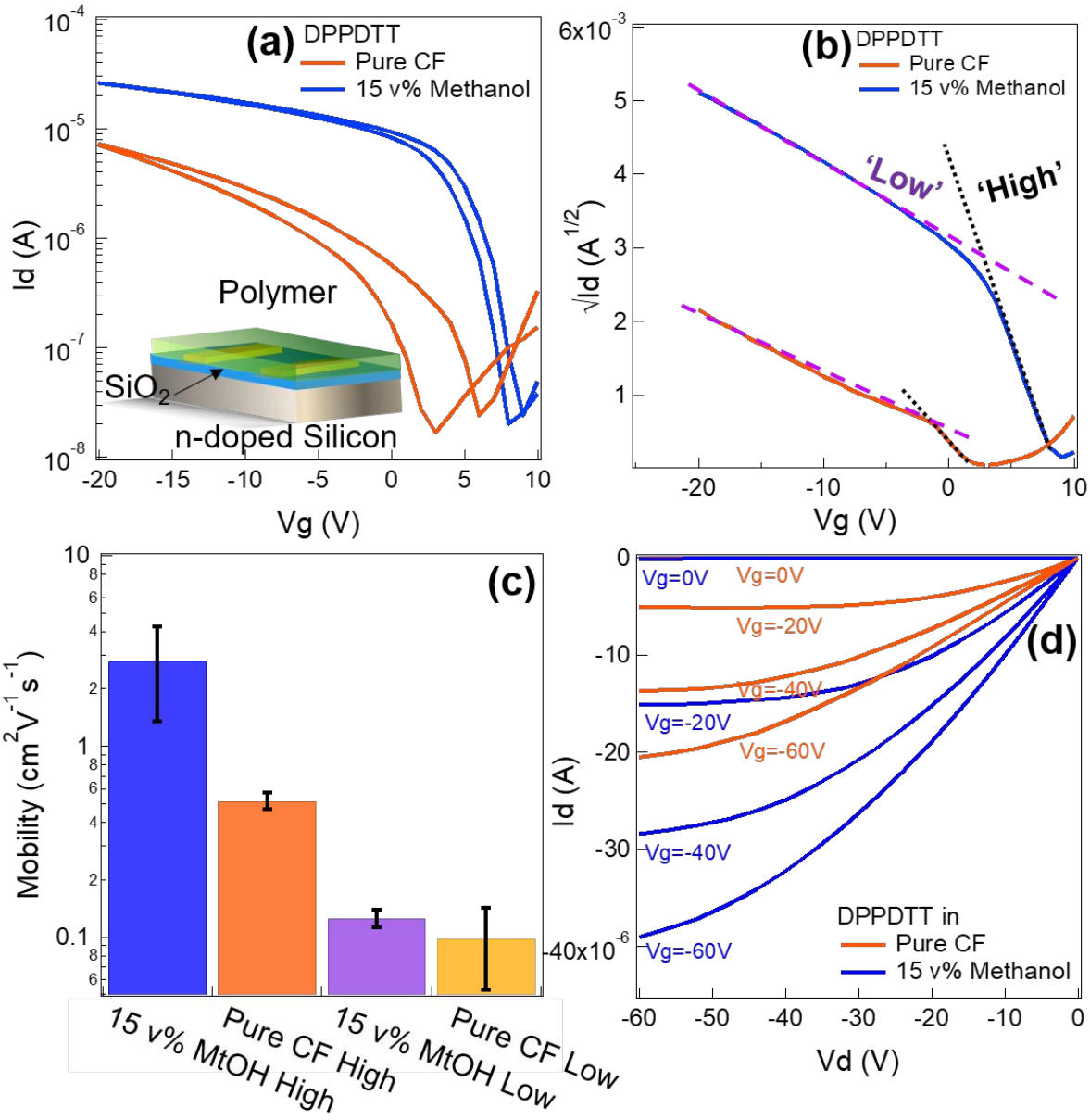

Figure 8. (a) Transfer curves for bottom-gate bottom-contact OFETs fabricated from DPPDTT dissolved in pure chloroform and with 15 v% methanol. The inset figure shows the device geometry. (b) Square root of current vs. gate voltage for two representative devices. The dashed lines represent the two fits ('High' and 'Low') that were used to obtain the mobility values.[53] (c) The average mobilities as estimated from the two different methods. The mobility was averaged from 10 devices for each condition. (d) Comparison of output curves from fully dissolved and self-assembled (15 v% methanol) polymers.

We also explored other donor-acceptor conjugated polymers in order to see if the same 'poor' solvent polarity dependence of self-assembly is observed. This analysis includes PCDTBT, PCDTPT, and PFT-100, where the molecular structures are depicted together with DPPDTT in Figure 9. The surface morphology of films formed after addition of methanol and n-hexane are also characterized with AFM and are shown in Figure 10. With the addition of n-hexane, the films are relatively flat and uniform. In comparison, the same amount of methanol (polar) shows clear signs of induced self-assembly into large aggregates. For samples composed of PFT-100, short nanoribbons were formed that are micrometers long and less than 50 nm in width. It is important to note that the polymer structures of PCDTPT and PFT-100 are very similar and only differ in the areas shown in dashed circles in Figure 9.

Although it is possible that the change in nanostructure resulted from this small change in molecular composition, the polymer concentration (c(PCDTPT)=3.2 mg/ml, c(PFT-100)=1.6 mg/ml), molecular weight (M_w(PCDTPT)=76k, M_w(PFT-100)=50k) and polydispersity (*Đ(PCDTPT)=2.5, Đ(PFT-100)=3*) of the polymers may all play additional roles. Therefore, we cannot conclude that these differences arise from any one of the above reasons and additional work is needed to illuminate this further. On the other hand, we have conclusively demonstrated that mixtures of solvents can strongly affect the formation of nanostructures for other DACPs.

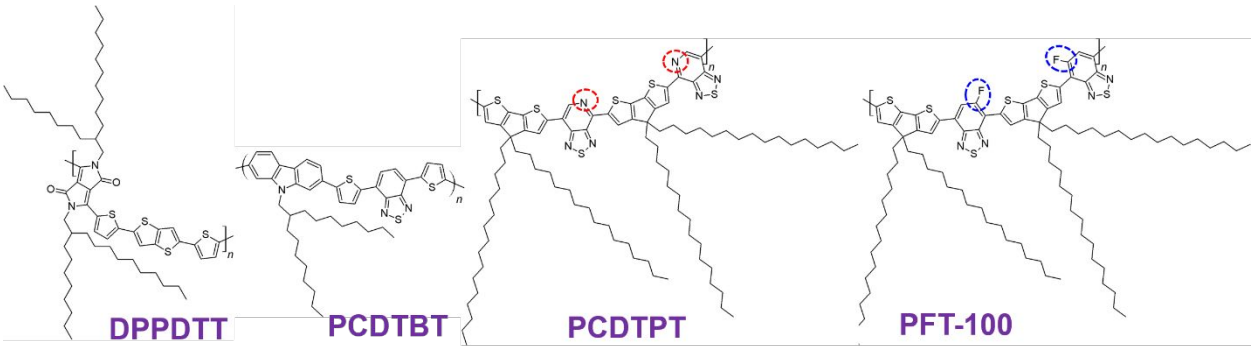

Figure 9. The schematic drawing of molecular structures of DPPDTT, PCDTPT, PFT-100, and PCDTBT.

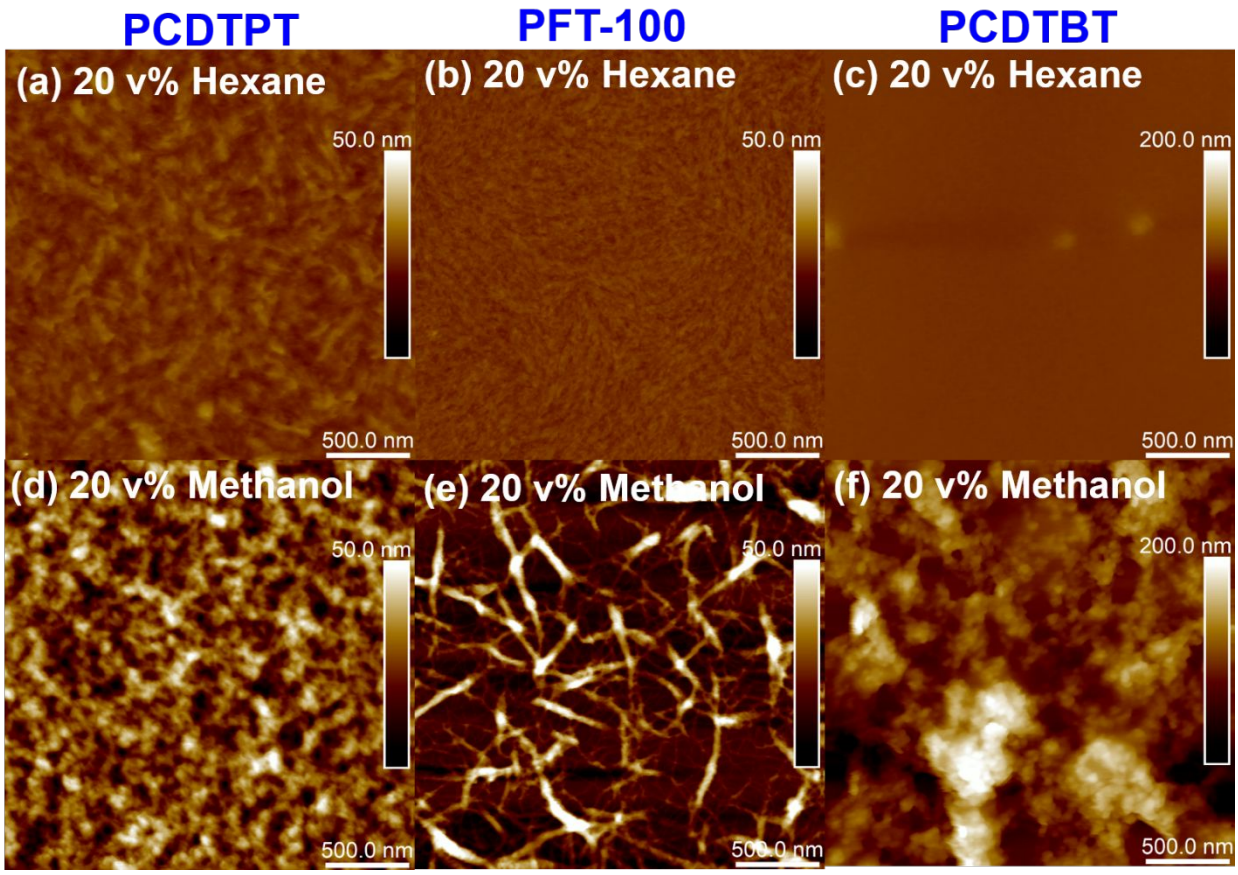

Figure 10. AFM images of structure formed from three different donor-acceptor conjugated polymers by mixing 20 v% (a) (b) (c) n-hexane and 20 v% (d) (e) (f) methanol.

Discussions:

Donor-acceptor conjugated polymers (DACPs) are shown to form ordered nanoribbons by mixing polar 'poor' solvents into stable solutions in 'good' solvents. It is hypothesized that addition of 'poor' solvents effectively reduces the solubility of DA polymers and induces aggregation in solution. However, unlike for conjugated homopolymers, it is clear that the polarity of the added

solvents is an important parameter for inducing controlled self-assembly vs. aggregation. The addition of polar 'poor' solvents (e.g. methanol) to a 'good' solvent (i.e. chloroform) for DACPs leads to the formation of nanoribbons. In contrast, the same DACPs form disordered aggregates when samples in chloroform are mixed with non-polar 'poor' solvents (e.g. n-hexane).

We hypothesize that, when polar 'poor' solvents are added to polymer solutions in chloroform, the dipole within the polar solvent molecules may interact with the backbone of the DA polymer. Dipole-dipole interactions between the solvent molecules and the alternating electron-rich and electron-deficient subunits in the backbone may play a key role in facilitating the formation of π-π stacking interactions in solution, which is not easily achieved for DACPs due to their complex backbone architecture. Crystallization and growth due to the reduced solubility eventually leads to the formation of large and organized nanoribbons spanning over very long distances (Figure 1 and Figure 5). In contrast, the addition of non-polar 'poor' solvents (e.g. n-hexane) to chloroform reduces DACP solubility but does not lead to a preferred orientation for assembly. These aggregates were observed to have amorphous shapes as shown in Figure 3 and Figure 5.

The difference in the structures that would form when either polar or nonpolar 'poor' solvents were added to chloroform was also observed for several other DACPs (Figure 10). It is worth mentioning that the solvent-polymer interactions are likely not limited to dipole-dipole interactions. Hydrogen bonding may also play a key role in forming the observed ordered structures in DACPs. Experimental and computational research with techniques of high molecular resolution will be needed in order to fully uncover the role of solvent composition on the formation of nanoribbons in DACPs.

The addition of 'poor' solvents to chloroform also leads to conformational changes of polymers in solution well before they assemble into larger structures. This is evidenced by the SANS data in

Figure 2 that characterizes dilute DACP solutions. The Kuhn length, which is a measure of the rigidity of polymer chains in solution, slightly increased from 30.2 nm to 35.3 nm with 5 v% methanol addition for DPPDTT. Further addition of methanol to chloroform exceeding 15 v% increased the radius and length of the cylinder, but not the Kuhn length, indicating that polymers started to assemble into large structures. Interestingly, similar change in stiffness of the DACP chains is also observed with addition of the non-polar solvent n-hexane to chloroform (Figure S8 in the Supporting Information), even though it would not result in the formation of large-scale ordered structures. Although changes in the contour length of DPPDTT dissolved chains may also be extracted from the collected SANS data, the resolution of the instrument was inadequate to accurately measure this parameter for these samples due to the high molecular weight and stiffness of this polymer (279 kg/mol).

Similar conformation changes were also observed with a different DA polymer PCDTPT when a polar 'poor' solvent (e.g. methanol) was added to a sample dissolved in a 'good' solvent (i.e. chloroform). A semi-flexible cylinder model was used to fit the SANS data in dissolved state as shown in Figure 11. The addition of methanol also led to an increase of radius and the contour length of the cylinder (Table 2). At the same time, Kuhn length of the polymer reduced after they started to assemble, which was also observed in DPPDTT polymer (Figure 2). In the fitting of PCDTPT in pure chloroform, the Kuhn length was slightly larger than the contour length of the polymer. Forcing the Kuhn length to be the same value as contour length barely affected the fit quality (i.e. χ^2 parameter changed from 3.27 to 3.29).

SANS results for DPPDTT and PCDTPT suggest a much stiffer backbone for DACPs in comparison to that of conjugated homopolymers like P3HT and PFO. For the shorter PCDTPT chains, it was even possible to fit the SANS data with a perfectly rigid cylinder (rigid rod) model,

as shown in Figure S9 and Table S2 in the supporting information. The Kuhn length of DPPDTT (30.2 nm) and PCDTPT (30.9 nm), even when dissolved in the 'good' solvent chloroform, were found to be about five times larger than that of P3HT (~6 nm). [27,28] The higher rigidity of donor-acceptor polymers might contribute to the different solution-phase assembly that is observed when compared to the well-known and characterized P3HT nanowire formation. It is clear that the addition of methanol (polar 'poor' solvent) to polymer solution in chloroform has a profound effect on the conformation of DACPs in solution and that it serves as an effective 'trigger' for self-assembly to occur. The importance of polar and ionic interactions in solutions of DACPs is further supported by theoretical calculations in recent reports stating that incorporation of small amounts of ionic liquids (polar) into DPPDTT solutions was found to hinder side-chain torsion and this facilitated the formation of ordered chain stacks. [6]

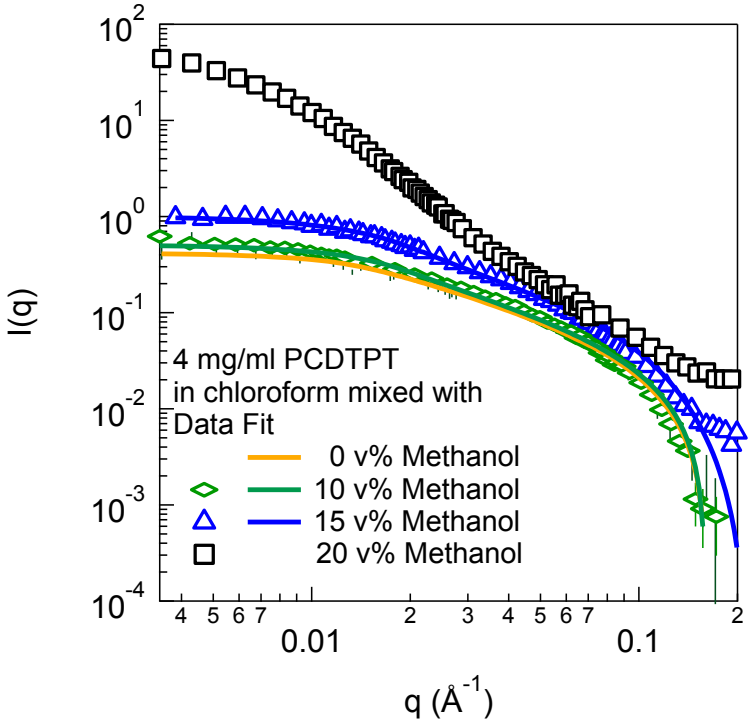

Figure 11. 1D SANS scattering profile of 4 mg/ml PCDTPT in chloroform mixed with varied methanol concentrations. A semi-flexible cylinder model was used to fit the SANS profiles at low methanol concentrations.

Table 2. Radius, Kuhn Length, and Contour Length of PCDTPT extrapolated from flexible cylinder model as a function of methanol ratio.

.

Methanol Ratio	Radius (nm)	Kuhn Length (nm)	Contour Length (nm)
0 v%	1.5	30.9	27.8
10 v%	1.4	20.8	31.5
15 v%	1.7	18.8	37.3

Unlike whiskers formed in P3HT and other homopolymers, nanoribbons were not observed by addition of n-hexane for any DA polymer. Instead, large aggregates were formed that could be observed in AFM images for all polymers investigated in Figure 3 and Figure 10. Therefore, the solubility of a DACP cannot be the sole parameter that determines the macromolecular structures that are formed in solution. In contrast, by reducing the solubility of P3HT to a critical limit using nonpolar solvents (e.g. n-hexane or dodecane) nanofiber formation is easily achieved. [13,19,23] For DACPs, it is interesting to find that the fraction of polymers that would form nanoribbons and the cross-sectional size of the ribbons could vary significantly depending on specific polymer-solvent interactions (Table 1). For P3HT, the cross-sectional size of the nanowires stays relative constant when different solvents are used. [11,23] Even though addition of polar 'poor' solvents to DACPs dissolved in chloroform promotes the formation of nanoribbons that appear similar to P3HT nanowires, it is important to note that there are differences between these structures. P3HT has been reported to form both nanoribbons and nanowires depending on the conditions used for self-assembly [11,16]Although these structures may appear to be similar, P3HT nanoribbons grow with a different crystal orientation when compared to nanofibers. Nanoribbons grow along (100)

direction while nanofibers grow along (010) direction.[16] In addition, the generation of nanoribbons is rare for P3HT in comparison to nanofibers, since it requires careful control of self-assembly conditions.

The modification of solvent quality for DACPs was found to also affect the polymer chain packing in solid films. GIWAXS results show that 'poor' solvents with different polarities could change the crystal orientation with respect to the substrates. With the addition of polar 'poor' solvents (i.e. methanol, DMSO, and ACN) to chloroform, the π-π stacking peak became randomly oriented with respect to the substrate (Figure 4 and Figure 7). In contrast, the addition of the nonpolar 'poor' solvent n-hexane promoted the in-plane crystal arrangement. Since different organic electronic devices require charge transport in different directions (i.e. OFET vs. OPV), changing the solvents used to induce assembly may provide a facile route for fine tuning and optimizing charge transport to enhance device performance.

The molecular interactions between solvent molecules in mixtures may also be important in directing the formation of nanostructures in DACPs. Neither methanol nor n-hexane form molecularly homogeneous mixtures with chloroform. This can be observed in SANS scattering profiles for solvent mixtures (i.e. no polymer) at high-q in Figure S10 in the Supporting Information. A 'hump' is observed at very high-q after methanol or n-hexane addition to chloroform. Fits to spherical form factors revealed a radius of ~ 4.3 Å of methanol and ~ 3.5 Å of hexane dispersed in chloroform. In contrast, DMSO and ACN are completely miscible with chloroform and showed a fully flat background at high q values.

Since DACPs have complex molecular structures when compared to homopolymers, more factors need to take into account for self-assembly besides solubility, such as polymer-solvent and polymer-polymer interactions. Single-chain conformation in solution needs to be further

investigated to better understand the molecular mechanisms that cause differences in self-assembly through solvent polarity. Recently, Tenopala-Carmona et al. demonstrated experimental observations of real-time single-chain conformations in solution based on single-molecule fluorescence microscopy for conjugated polymers.[55] In addition, molecular dynamics (MD) simulations could be performed with both polar and nonpolar explicit solvents to further understand the molecular and topological details of their interactions with DACPs. This could further shine light on the polymer chain conformation and spatial distribution of solvent molecules around polymer chains, which could facilitate the understanding of how solvent-polymer interactions evolve in mixed solvents. Also, MD simulations can be implemented to provide molecular understanding of polymer-polymer interactions occurring during solution crystallization processes. In fact, a couple of groups have started to investigate DACP packing by coupling MD simulations with experimental techniques, such as GIWAXS or nuclear magnetic resonance (NMR).[33,34]

Conclusions:

The self-assembly of donor-acceptor conjugated polymers into nanoribbons is induced by the addition of certain miscible polar 'poor' solvents to dilute solutions in the 'good' solvent chloroform. The polarity of the 'poor' solvent additive was found to be an important parameter for this self-assembly process to occur. The use of non-polar 'poor' solvents to induce aggregation resulted in aggregates with amorphous shapes. For 'poor' solvents with varied polarity, changes in the chain rigidity (Kuhn length) of DACPs were observed in dilute solutions prior to self-assembly. The interactions between 'poor' solvent molecules and polymers, as well as those between 'poor' solvent and 'good' solvent molecules were both important in determining the

resulting polymer structure and chain packing. An enhancement of hole mobility in OFETs resulted from the formation of nanostructures upon addition of the polar solvent methanol to DACP solutions in chloroform. The self-assembly of DACPs by addition of polar 'poor' solvents to samples dissolved in 'good' solvents (i.e. chloroform) was found to be a promising method to improving the performance of these materials.

Acknowledgements:

The research was primarily funded by the Department of Energy, Office of Basic Energy Sciences under award number DE-SC0010282. We appreciate the support from NIST Center for Neutron Research (NCNR) for providing neutron research facilities. The GIWAXS experiments were conducted at Advanced Photon Source operated by Argonne National Laboratory, a U.S. Department of Energy (DOE) Office of Science User Facility, under Contract No. DE-AC02-06CH11357. The authors acknowledge the help from Dr. David S. Li and Yi-Ting Lee for implementing GIWAXS and SANS experiments, Dylan G. Karis for GPC measurement of PCDTBT, as well as Dr. Jeffrey J. Richards for conducting impedance measurements on nanoribbon dispersions. The authors thank Craig Brown and Joseph R. Kline at NIST for helpful discussions and suggestions on interpreting GIWAXS data. Part of the characterization was performed at the Molecular Analysis Facility (MAF) in the Molecular Engineering & Sciences Institute, which is supported by the National Nanotechnology Coordinated Infrastructure (NNCI-1542101).

REFERENCES

(1) Shin, H.; Seo, S.; Park, C.; Na, J.; Han, M.; Kim, E. Energy Saving Electrochromic Windows from Bistable Low-HOMO Level Conjugated Polymers. *Energy Environ. Sci.* **2016**, *9* (1), 117–122 DOI: 10.1039/C5EE03160E.

(2) Simon, D. T.; Gabrielsson, E. O.; Tybrandt, K.; Berggren, M. Organic Bioelectronics: Bridging the Signaling Gap between Biology and Technology. *Chem. Rev.* **2016**, *116* (21), 13009–13041 DOI: 10.1021/acs.chemrev.6b00146.

(3) Chortos, A.; Liu, J.; Bao, Z. Pursuing Prosthetic Electronic Skin. *Nat. Mater.* **2016**, No. July, 1–14 DOI: 10.1038/nmat4671.

(4) Wu, C.-H.; Chueh, C.-C.; Xi, Y.-Y.; Zhong, H.-L.; Gao, G.-P.; Wang, Z.-H.; Pozzo, L. D.; Wen, T.-C.; Jen, A. K.-Y. Influence of Molecular Geometry of Perylene Diimide Dimers and Polymers on Bulk Heterojunction Morphology Toward High-Performance Nonfullerene Polymer Solar Cells. *Adv. Funct. Mater.* **2015**, *25* (33), 5326–5332 DOI: 10.1002/adfm.201501971.

(5) Luo, C.; Kyaw, K. K.; Perez, L. a; Patel, S.; Wang, M.; Grimm, B.; Bazan, G. C.; Kramer, E. J.; Heeger, A. J. General Strategy for Self-Assembly of Highly Oriented Nanocrystalline Semiconducting Polymers with High Mobility. *Nano Lett.* **2014**, *14*, 2764 DOI: 10.1021/nl500758w.

(6) Luo, H.; Yu, C.; Liu, Z.; Zhang, G.; Geng, H.; Yi, Y.; Broch, K.; Hu, Y.; Sadhanala, A.; Jiang, L.; Qi, P.; Cai, Z.; Sirringhaus, H.; Zhang, D. Remarkable Enhancement of Charge Carrier Mobility of Conjugated Polymer Field-Effect Transistors upon Incorporating an Ionic Additive. *Sci. Adv.* **2016**, *2* (May), e1600076 DOI: 10.1126/sciadv.1600076.

(7) Li, J.; Zhao, Y.; Tan, H. S.; Guo, Y.; Di, C.-A.; Yu, G.; Liu, Y.; Lin, M.; Lim, S. H.; Zhou, Y.; Su, H.; Ong, B. S. A Stable Solution-Processed Polymer Semiconductor with Record High-Mobility for Printed Transistors. *Sci. Rep.* **2012**, *2*, 754 DOI: 10.1038/srep00754.

(8) Müllen, K.; Pisula, W. Donor–Acceptor Polymers. *J. Am. Chem. Soc.* **2015**, *137* (30), 9503–9505 DOI: 10.1021/jacs.5b07015.

(9) Noriega, R.; Rivnay, J.; Vandewal, K.; Koch, F. P. V.; Stingelin, N.; Smith, P.; Toney, M. F.; Salleo, A. A General Relationship between Disorder, Aggregation and Charge Transport in Conjugated Polymers. *Nat. Mater.* **2013**, *12* (11), 1038–1044 DOI: 10.1038/nmat3722.

(10) Street, R. A. Unraveling Charge Transport in Conjugated Polymers. *Science (80-.).* **2013**, *341* (6150), 1072–1073 DOI: 10.1126/science.1242935.

(11) Newbloom, G. M.; Kim, F. S.; Jenekhe, S. a.; Pozzo, D. C. Mesoscale Morphology and Charge Transport in Colloidal Networks of Poly(3-Hexylthiophene). *Macromolecules* **2011**, *44* (10), 3801–3809 DOI: 10.1021/ma2000515.

(12) Newbloom, G. M.; Weigandt, K. M.; Pozzo, D. C. Electrical, Mechanical, and Structural Characterization of Self-Assembly in Poly(3-Hexylthiophene) Organogel Networks. *Macromolecules* **2012**, *45*, 3452–3462 DOI: 10.1021/ma202564k.

(13) Newbloom, G. M.; de la Iglesia, P.; Pozzo, L. D. Controlled Gelation of Poly(3-Alkylthiophene)s in Bulk and in Thin-Films Using Low Volatility Solvent/Poor-Solvent Mixtures. *Soft Matter* **2014**, *10* (44), 8945–8954 DOI: 10.1039/c4sm00960f.

(14) Xi, Y.; Pozzo, L. D. Electric Field Directed Formation of Aligned Conjugated Polymer

Fibers. *Soft Matter* **2017**, *13*, 3894–3908 DOI: 10.1039/C7SM00485K.
(15) Li, J.-H.; Xi, Y.; Pozzo, L. D.; Xu, J.-T.; Luscombe, C. K. Macroscopically Aligned Nanowire Arrays of π-Conjugated Polymers via Shear-Enhanced Crystallization. *J. Mater. Chem. C* **2017**, *5* (21), 5128–5134 DOI: 10.1039/C7TC01419H.
(16) Liu, J.; Arif, M.; Zou, J.; Khondaker, S. I.; Zhai, L. Controlling Poly(3-Hexylthiophene) Crystal Dimension: Nanowhiskers and Nanoribbons. *Macromolecules* **2009**, *42* (24), 9390–9393 DOI: 10.1021/ma901955c.
(17) Kiriy, N.; Jähne, E.; Adler, H. J.; Schneider, M.; Kiriy, A.; Gorodyska, G.; Minko, S.; Jehnichen, D.; Simon, P.; Fokin, A. A.; Stamm, M. One-Dimensional Aggregation of Regioregular Polyalkylthiophenes. *Nano Lett.* **2003**, *3* (6), 707–712 DOI: 10.1021/nl0341032.
(18) Han, Y.; Guo, Y.; Chang, Y.; Geng, Y.; Su, Z. Chain Folding in Poly(3-Hexylthiophene) Crystals. *Macromolecules* **2014**, *47* (11), 3708–3712 DOI: 10.1021/ma5006149.
(19) Chang, M.; Choi, D.; Fu, B.; Reichmanis, E. Solvent Based Hydrogen Bonding: Impact on Poly(3-Hexylthiophene) Nanoscale Morphology and Charge Transport Characteristics. *ACS Nano* **2013**, *7* (6), 5402–5413 DOI: 10.1021/nn401323f.
(20) Zhu, Z.; Wei, B.; Wang, J. Self-Assembly of Poly(3-Hexylthiophene) Nanowire Networks by a Mixed-Solvent Approach for Organic Field-Effect Transistors. *Phys. Status Solidi - Rapid Res. Lett.* **2014**, *8* (3), 252–255 DOI: 10.1002/pssr.201308270.
(21) Kiymaz, D.; Yagmurcukardes, M.; Tomak, A.; Sahin, H.; Senger, R. T.; Peeters, F. M.; Zareie, H. M.; Zafer, C. Controlled Growth Mechanism of Poly (3-Hexylthiophene) Nanowires. *Nanotechnology* **2016**, *27* (45), 455604 DOI: 10.1088/0957-4484/27/45/455604.
(22) Scharsich, C.; Lohwasser, R. H.; Sommer, M.; Asawapirom, U.; Scherf, U.; Thelakkat, M.; Neher, D.; Köhler, A. Control of Aggregate Formation in Poly(3-Hexylthiophene) by Solvent, Molecular Weight, and Synthetic Method. *J. Polym. Sci. Part B Polym. Phys.* **2012**, *50* (6), 442–453 DOI: 10.1002/polb.23022.
(23) Keum, J. K.; Xiao, K.; Ivanov, I. N.; Hong, K.; Browning, J. F.; Smith, G. S.; Shao, M.; Littrell, K. C.; Rondinone, A. J.; Andrew Payzant, E.; Chen, J.; Hensley, D. K. Solvent Quality-Induced Nucleation and Growth of Parallelepiped Nanorods in Dilute Poly(3-Hexylthiophene) (P3HT) Solution and the Impact on the Crystalline Morphology of Solution-Cast Thin Film. *CrystEngComm* **2013**, *15* (6), 1114–1124 DOI: 10.1039/c2ce26666k.
(24) Lim, G. H.; Zhuo, J. M.; Wong, L. Y.; Chua, S. J.; Chua, L. L.; Ho, P. K. H. A Transition Solvent Strategy to Print Polymer:Fullerene Films Using Halogen-Free Solvents for Solar Cell Applications. *Org. Electron. physics, Mater. Appl.* **2014**, *15* (2), 449–460 DOI: 10.1016/j.orgel.2013.10.025.
(25) Tan, B.; Pan, H.; Budhlall, B. M.; Sobkowicz, M. J. Poly(3-Hexylthiophene)/Poly(Styrene) Blended Colloids: Exploiting the Effects of Composition and Marginal Solvent. *Colloids Surfaces A Physicochem. Eng. Asp.* **2018**, *539* (December 2017), 221–228 DOI: 10.1016/j.colsurfa.2017.12.027.
(26) Kim, S.; Lee, W. H.; Mun, J.; Lee, H. S.; Park, Y. D. Marginal Solvents Preferentially Improve the Molecular Order of Thin Polythiophene Films. *RSC Adv.* **2016**, *6* (28), 23640–23644 DOI: 10.1039/c6ra00504g.
(27) McCulloch, B.; Ho, V.; Hoarfrost, M.; Stanley, C.; Do, C.; Heller, W. T.; Segalman, R. A. Polymer Chain Shape of Poly(3-Alkylthiophenes) in Solution Using Small-Angle Neutron

Scattering. *Macromolecules* **2013**, *46* (5), 1899–1907 DOI: 10.1021/ma302463d.
(28) Newbloom, G. M.; Hoffmann, S. M.; West, A. F.; Gile, M. C.; Sista, P.; Cheung, H.-K. C.; Luscombe, C. K.; Pfaendtner, J.; Pozzo, L. D. Solvatochromism and Conformational Changes in Fully Dissolved Poly(3-Alkylthiophene)S. *Langmuir* **2015**, *31* (1), 458–468 DOI: 10.1021/la503666x.
(29) Iglesia, P. D. La; Pozzo, D. C. Effects of Supersaturation on the Structure and Properties of Poly(9,9-Dioctyl Fluorene) Organogels. *Soft Matter* **2013**, *9* (47), 11214 DOI: 10.1039/c3sm51753e.
(30) Xi, Y.; Li, D. S.; Newbloom, G. M.; Tatum, W. K.; O'Donnell, M.; Luscombe, C. K.; Pozzo, L. D. Sonocrystallization of Conjugated Polymers with Ultrasound Fields. *Soft Matter* **2018**, *14* (24), 4963–4976 DOI: 10.1039/C8SM00905H.
(31) Brinkmann, M.; Gonthier, E.; Bogen, S.; Tremel, K.; Ludwigs, S.; Hufnagel, M.; Sommer, M. Segregated versus Mixed Interchain Stacking in Highly Oriented Films of Naphthalene Diimide Bithiophene Copolymers. *ACS Nano* **2012**, *6* (11), 10319–10326 DOI: 10.1021/nn304213h.
(32) Zheng, Y.-Q.; Yao, Z.-F.; Lei, T.; Dou, J.-H.; Yang, C.-Y.; Zou, L.; Meng, X.; Ma, W.; Wang, J.-Y.; Pei, J. Unraveling the Solution-State Supramolecular Structures of Donor-Acceptor Polymers and Their Influence on Solid-State Morphology and Charge-Transport Properties. *Adv. Mater.* **2017**, *1701072*, 1701072 DOI: 10.1002/adma.201701072.
(33) Niedzialek, D.; Lemaur, V.; Dudenko, D.; Shu, J.; Hansen, M. R.; Andreasen, J. W.; Pisula, W.; Müllen, K.; Cornil, J.; Beljonne, D. Probing the Relation between Charge Transport and Supramolecular Organization down to Ångström Resolution in a Benzothiadiazole- Cyclopentadithiophene Copolymer. *Adv. Mater.* **2013**, *25* (13), 1939–1947 DOI: 10.1002/adma.201201058.
(34) Chaudhari, S. R.; Griffin, J. M.; Broch, K.; Lesage, A.; Lemaur, V.; Dudenko, D.; Olivier, Y.; Sirringhaus, H.; Emsley, L.; Grey, C. P. Donor–acceptor Stacking Arrangements in Bulk and Thin-Film High-Mobility Conjugated Polymers Characterized Using Molecular Modelling and MAS and Surface-Enhanced Solid-State NMR Spectroscopy. *Chem. Sci.* **2017**, *8* (4), 3126–3136 DOI: 10.1039/C7SC00053G.
(35) Marszalek, T.; Li, M.; Pisula, W. Design Directed Self-Assembly of Donor–acceptor Polymers. *Chem. Commun.* **2016**, *52* (73), 10938–10947 DOI: 10.1039/C6CC04523E.
(36) Chen, M. S.; Lee, O. P.; Niskala, J. R.; Yiu, A. T.; Tassone, C. J.; Schmidt, K.; Beaujuge, P. M.; Onishi, S. S.; Toney, M. F.; Zettl, A.; Fréchet, J. M. J. Enhanced Solid-State Order and Field-Effect Hole Mobility through Control of Nanoscale Polymer Aggregation. *J. Am. Chem. Soc.* **2013**, *135* (51), 19229–19236 DOI: 10.1021/ja4088665.
(37) Ferdous, S.; Liu, F.; Wang, D.; Russell, T. P. Solvent-Polarity-Induced Active Layer Morphology Control in Crystalline Diketopyrrolopyrrole-Based Low Band Gap Polymer Photovoltaics. *Adv. Energy Mater.* **2014**, *4* (2), 1–10 DOI: 10.1002/aenm.201300834.
(38) Jiang, Z.; Li, X.; Strzalka, J.; Sprung, M.; Sun, T.; Sandy, A. R.; Narayanan, S.; Lee, D. R.; Wang, J. The Dedicated High-Resolution Grazing-Incidence X-Ray Scattering Beamline 8-ID-E at the Advanced Photon Source. *J. Synchrotron Radiat.* **2012**, *19* (4), 627–636 DOI: 10.1107/S0909049512022017.
(39) Jiang, Z. GIXSGUI : A MATLAB Toolbox for Grazing-Incidence X-Ray Scattering Data Visualization and Reduction, and Indexing of Buried Three-Dimensional Periodic Nanostructured Films. *J. Appl. Crystallogr.* **2015**, *48* (3), 917–926 DOI: 10.1107/S1600576715004434.

(40) Glinka, C. J.; Barker, J. G.; Hammouda, B.; Krueger, S.; Moyer, J. J.; Orts, W. J. The 30 m Small-Angle Neutron Scattering Instruments at the National Institute of Standards and Technology. *J. Appl. Crystallogr.* **1998**, *31* (3), 430–445 DOI: 10.1107/S0021889897017020.
(41) Kline, S. R. Reduction and Analysis of SANS and USANS Data Using IGOR Pro. *J. Appl. Crystallogr.* **2006**, *39* (6), 895–900 DOI: 10.1107/S0021889806035059.
(42) P. Butler, G. Alina, R. C. Hernandez, M. Doucet, A. Jackson, P. Kienzle, S. K. and J. Z. SASView for Small Angle Scattering Analysis http://www.sasview.org/.
(43) Chen, W.-R.; Butler, P. D.; Magid, L. J. Incorporating Intermicellar Interactions in the Fitting of SANS Data from Cationic Wormlike Micelles. *Langmuir* **2006**, *22* (15), 6539–6548 DOI: 10.1021/la0530440.
(44) Pedersen, J. S.; Schurtenberger, P. Scattering Functions of Semiflexible Polymers with and without Excluded Volume Effects. *Macromolecules* **1996**, *29* (23), 7602–7612 DOI: 10.1021/ma9607630.
(45) P. Mittelbach, G. P. X-Ray Low-Angle Scattering by Dilute Scattering Colloidal Systems. The Calculation of Scattering Curves of Parallelepipeds. *Acta Phys. Austriaca* **1961**, *14*, 185–211.
(46) Roman Nayuk, K. H. Formfactors of Hollow and Massive Rectangular Parallelepipeds at Variable Degree of Anisometry. *Zeitschrift für Phys. Chemie* **2012**, *226*, 837–854.
(47) H. Benoit. La Diffusion de La Lumiere Par Des Macromolecules En Chaines En Solution Dans Un Bon Solvant. *Comptes Rendus* **1957**, *245*, 2244–2247.
(48) Hammouda, B. SANS from Homogeneous Polymer Mixtures - A Unified Overview. *Adv. Polym. Sci.* **1993**, *106*, 87–133.
(49) Xi, Y.; Li, D. S.; Newbloom, G. M.; Tatum, W. K.; O'Donnell, M.; Luscombe, C. K.; Pozzo, L. D. Sonocrystallization of Conjugated Polymers with Ultrasound Fields. *Soft Matter* **2018**, *14* (24), 4963–4976 DOI: 10.1039/C8SM00905H.
(50) Egginger, M.; Bauer, S.; Schwödiauer, R.; Neugebauer, H.; Sariciftci, N. S. Current versus Gate Voltage Hysteresis in Organic Field Effect Transistors. *Monatshefte für Chemie - Chem. Mon.* **2009**, *140* (7), 735–750 DOI: 10.1007/s00706-009-0149-z.
(51) Lei, Y.; Deng, P.; Li, J.; Lin, M.; Zhu, F.; Ng, T.; Lee, C.; Ong, B. S. Solution-Processed Donor-Acceptor Polymer Nanowire Network Semiconductors For High-Performance Field-Effect Transistors. *Sci. Rep.* **2016**, *6* (1), 24476 DOI: 10.1038/srep24476.
(52) Phan, H.; Ford, M. J.; Lill, A. T.; Wang, M.; Bazan, G. C.; Nguyen, T.-Q. Electrical Double-Slope Nonideality in Organic Field-Effect Transistors. *Adv. Funct. Mater.* **2018**, *28* (17), 1707221 DOI: 10.1002/adfm.201707221.
(53) Choi, H. H.; Cho, K.; Frisbie, C. D.; Sirringhaus, H.; Podzorov, V. Critical Assessment of Charge Mobility Extraction in FETs. *Nat. Mater.* **2017**, *17* (1), 2–7 DOI: 10.1038/nmat5035.
(54) Lei, Y.; Deng, P.; Zhang, Q.; Xiong, Z.; Li, Q.; Mai, J.; Lu, X.; Zhu, X.; Ong, B. S. Hydrocarbons-Driven Crystallization of Polymer Semiconductors for Low-Temperature Fabrication of High-Performance Organic Field-Effect Transistors. *Adv. Funct. Mater.* **2018**, *28* (15), 1–9 DOI: 10.1002/adfm.201706372.
(55) Tenopala-Carmona, F.; Fronk, S.; Bazan, G. C.; Samuel, I. D. W.; Penedo, J. C. Real-Time Observation of Conformational Switching in Single Conjugated Polymer Chains. *Sci. Adv.* **2018**, *4* (2), eaao5786 DOI: 10.1126/sciadv.aao5786.

Table of Contents

Self-assembly of Donor-acceptor Conjugated Polymers Induced by Miscible 'Poor' Solvents

Yuyin Xi†, Caitlyn M. Wolf, and Lilo D. Pozzo*

Department of Chemical Engineering, University of Washington, Seattle, WA 98195

* Email: dpozzo@uw.edu

† Current address:

Center for Neutron Research, National Institute of Standards and Technology, Gaithersburg, MD, 20899, USA

Department of Chemical and Biomolecular Engineering, University of Delaware, Newark, DE, 19716, USA

Polarity of 'poor' solvent strongly affects the structure of self-assembled donor-acceptor conjugated polymers